Letters

IOP Publishing

Journal of Physics D: Applied Physics

J. Phys. D: Appl. Phys. **53** (2020) 22LT01 (9pp)

https://doi.org/10.1088/1361-6463/ab7e64

Letter

A fan-shaped plasma reactor for mixing enhancement in a closed chamber

Sherlie Portugal[1,3], Bhaswati Choudhury[2], Alexander Lilley[2], Christopher Charters[2], Christian Porrello[2], Jenshan Lin[1] and Subrata Roy[2,4]

[1] Department of Electrical and Computer Engineering, University of Florida, Gainesville, United States of America

[2] Department of Mechanical and Aerospace Engineering, University of Florida, Gainesville, United States of America

[3] School of Electrical Engineering, Technological University of Panama, Panama City, Panama

[4] SurfPlasma Inc., Gainesville, FL 32601, United States of America

E-mail: roy@ufl.edu

Received 3 October 2019, revised 3 February 2020

Accepted for publication 10 March 2020

Published 1 April 2020

Abstract

This paper introduces a novel fan-shaped plasma reactor, which employs vortex-induced airflow by atmospheric dielectric barrier discharge to enhance mixing and the resulting distribution of the neighboring species of generated ozone. Through stereoscopic PIV and smoke flow visualizations it was demonstrated that mechanisms of suction, vortex creation and ejection of the fluid combine to form a vertical turbulent flow that yields a more controlled and uniform ozone distribution. The performance of the fan reactor was compared to that of a conventional comb reactor for three cross-sectional planes of a space volume simulating the decontamination environment. Results show that with the fan reactor, ozone starts spreading from the center of the plane, which makes the reactor itself responsible for most of the mixing and ozone's distribution pattern; whereas in the case of the comb reactor, mixing seems to be mostly dependent on the interaction between the reactor's characteristic flow and the boundaries of the space volume.

Keywords: cold plasma, ozone distribution, decontamination, plasma actuation, electrode design, surface DBD, fan reactor

(Some figures may appear in colour only in the online journal)

1. Introduction

Dielectric barrier discharge (DBD) plasma reactors operated in atmospheric air or pure oxygen produce ozone (O_3) as well as other reactive oxygen species (ROS) that can be employed in the microbial decontamination of objects and environments. Due to its high reactive molecular structure [1], O_3 is very effective in inactivating viruses and other microorganisms [1–5] and leaves minimal harmful footprints once it has been dissipated in air or water [6]. This makes it a very attractive solution for a wide variety of applications including certain hospital settings and the food industry—e.g. preserving grains and produce—where conventional methods of sterilization involving high temperature, steam or harsh chemicals cannot be utilized [7].

It has also been demonstrated that DBD reactors provide aerodynamic actuation that could mitigate issues like boundary layer separation, critical for stall control [8]. Subsequent studies using linear DBD reactors showed that the electrohydrodynamic (EHD) force induced by the momentum transfer between charged and neutral particles in the plasma region produces a wall jet with typical maximum velocities between 1 m s^{-1} to 10 m s^{-1} [9]. Besides linear electrodes, other geometries and arrays were proposed to exert specific

effects in the surrounding flow; worth mentioning examples are the round and square serpentine [10, 11], vortex generators [12], and synthetic jets [13].

The energy requirements to generate surface DBD (SDBD) plasma should not compromise the competitiveness and viability of ozone-based decontamination. Besides improving the design of electrical parts, one could aim to reduce the exposure time necessary to decontaminate subjects in a room or enclosure. The method proposed here is to use the energy naturally spent by SDBD reactors in flow generation to distribute the generated O_3. These reactors would employ their aerodynamic properties of SDBD actuators to better mix the generated ozone into the neighboring air, helping to disinfect/sterilize all points of an enclosure in a shorter period of time. Consequently, the required time of operation of electric circuits and plasma actuators would shorten, extending their total lifespan. One such design is a fan-shaped plasma reactor introduced in this paper and aimed to produce a fully three-dimensional turbulent flow that could enhance rapid mixing for more uniform ozone distribution in a small closed space. This particular fan shaped design is called *fan reactor* due to the close geometric resemblance of the electrodes to the blades of a fan.

2. Design of plasma reactors

2.1. Fan reactor

An illustration of the proposed fan reactor is shown in figure 1. The exposed electrode consists of five bent legs, hereafter identified as blades, each being a single copper strip of width w_e. Through the precise alignment of the covered electrode, as shown in figure 1(e), plasma forms only in specific regions along the edge of the blades that, for analysis purposes, are labeled as lines L_1, L_2, L_3 and L_4. The blades were designed so that lines L_1 and L_3 are located on the same radial axis to ensure maximum interaction of their induced flows. In addition, a horizontal gap g was added between exposed and covered electrode to avoid undesired plasma on external edges of the exposed electrode. The external circumference of the fan reactor with a radius r_o was set to be three times larger than the internal circumference with radius r_i. The length of L_1, L_3 and L_4 are given by $\varphi \times (r_o - w_e/2)$, $\varphi \times (r_i + w_e/2)$ and $\varphi \times (r_i - w_e/2)$, respectively; where $\varphi = 2\pi/10$ rad (36°). The length of L_2 depends on its radius of curvature, chosen arbitrarily to be approximately $r_o/2$, and the distance between L_1 and L_3. For the specific prototype used here, $r_o = 2.54$ cm (1 inch), $r_i = 0.85$ cm (1/3 inch) and $g = w_e = 1.27$ mm.

2.2. Comb reactor

To judge the performance of the fan reactor (Fan), a conventional comb shaped reactor (Comb) was used as reference. This reactor has been used often in previous plasma sterilizations studies [14, 15], and the reader is encouraged to resort to such publications for further details and analysis of its physical and electrical properties. The specific dimensions of the two prototypes used in this research are shown in figure 2. The smaller version, in figure 2(a), was used for the observation of the flow field due to the limited extension of the field of view of the PIV cameras; whereas the larger one, in figure 2(b), was used to obtain ozone information. Regardless of the size of the comb reactor, the flow pattern should remain consistent, with only maximum velocities differing, as demonstrated by other studies [16] and smoke visualization tests performed in the lab.

3. Experimental procedure

The techniques used to capture and analyze the flow pattern of the SDBD reactors were stereoscopic particle image velocimetry (stereo-PIV) [17] and smoke flow visualizations [18]. The stereo-PIV system used to obtain the average velocity vectors in the flow field used a Nd:YAG laser model Solo II-30 to produce a light beam with wavelength of 532 nm and high-speed CCD cameras model LaVision ImagerProX4M with a resolution of 2048 × 2048 pixels. The combination of the two cameras yielded de-warped images with resolution of 2059 × 2051 pixels and scale factor of 25.99°pixel mm^{-1}, which translate to a viewing area of approximately 79 × 79 mm. A total of 500 pairs of double-frame images were recorded per experiment. The cameras were operated at a double-frame mode, with repetition rate of 5 Hz and laser pulse separation (Δt) of 250 μs. The total maximum uncertainty, including both statistical and device error, was less than 5%. The correspondence between the de-warped image and the coordinates of the object plane in the stereoscopic PIV system had an RMS error 0.32°pixels for both cameras, with 2°pixels being an indication of poor correspondence and 0.3°pixels indicating an excellent fit. The quiescent chamber containing the reactor and seeding particles was made out of Polymethyl methacrylate (PMMA) with dimensions 1.207 m long × 0.597 m wide × 1.219 m high. Two cameras were placed on a heavy-duty camera track slider, controlled remotely with the aid of a stepping motor model PK268-03 from Oriental Motor U.S.A. Corp. The seeding particles were droplets of Shell Ondina Oil 917 vaporized with a TSI atomizer (Model 9302) pressurized at 25 psi.

The average velocity was obtained by studying the instantaneous behavior of the flow obtained through smoke flow visualizations. The smoke flow was recorded with a high-speed Phantom V7.3 camera at 1000 frames s^{-1} using and a Nikon 50 mm lens. A low-power 1 W laser with wavelength of 465 nm and a cylindrical diverging lens were used to generate a continuous light sheet to illuminate the seeding particles, which consisted of a fog juice composed of 1:5 glycerin to water ratio. These experiments were performed in a smaller quiescent chamber with dimensions 0.61 m × 0.61 m × 1.2 m.

To test the influence of the two distinct electrode designs, namely the Fan and the Comb, on O_3 distribution, the reactors were placed inside a custom polycarbonate box with internal dimensions 27.3 cm long × 27.3 cm wide × 28.6 cm high and wall thickness of 1.27 cm. A silicon layer was placed between the lid and sidewalls of the box to seal it from the external environment. The evolution of O_3 was observed on a two-dimensional (2D) grid of 36 measurement points, equivalent to

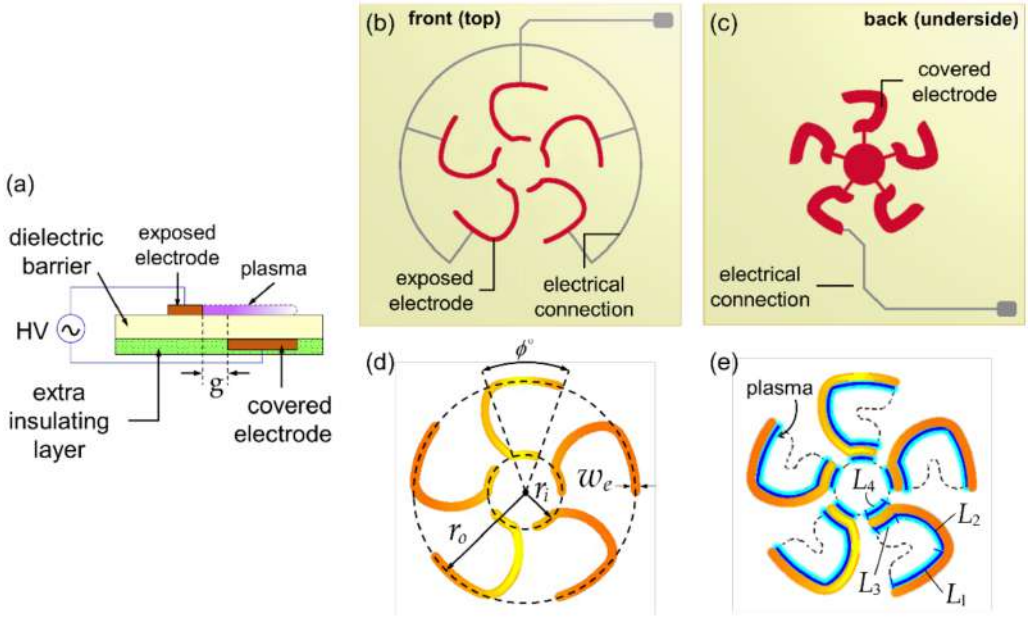

Figure 1. (a) SDBD principle. (b) Front (top) of the fan reactor. (c) Back (underside) of the fan reactor. (d) Geometrical parameters of the exposed electrode. (e) Segments along the edge of the expose electrode where plasma is formed due to the influence of the covered electrode, presented in dashed lines to indicate that it is located on a different plane.

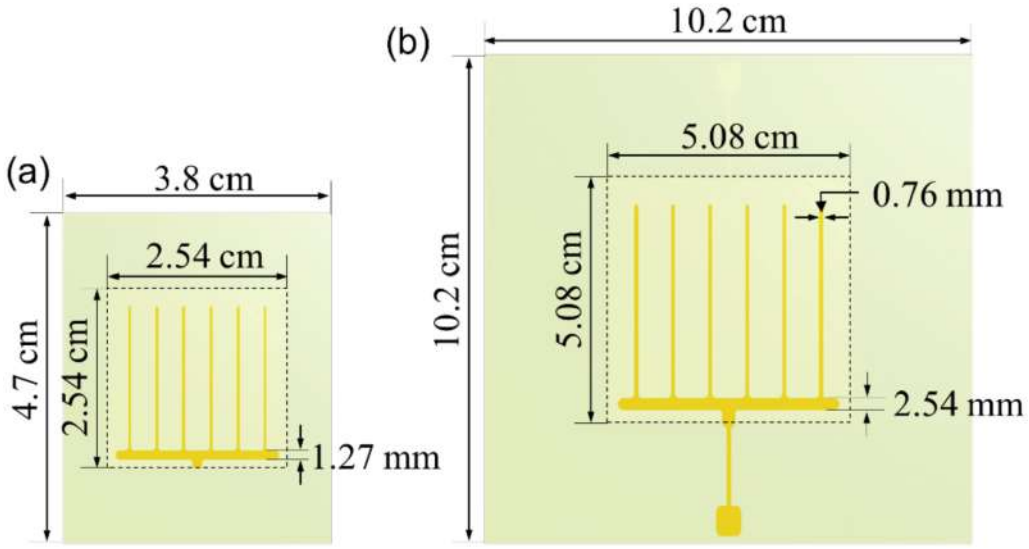

Figure 2. Comb reactor. (a) Smaller version used in the observation of the air flow. (b) Larger version used in the collection of ozone data and smoke flow visualizations.

horizontal cross-sectional planes in the internal space volume as shown in figure 3. Three planes were studied: Plane 1 (P1), Plane 2 (P2) and Plane 3 (P3) positioned at 3.5 cm, 11.5 cm and 18.5 cm from the bottom of the box, respectively. The reactor under test lay on the surface of the chamber's floor at the center location, which according to the (Q,R) coordinate system in figure 3 corresponds to the point $(3.5, 3.5)$. The orientations of the comb and fan reactors in the enclosure are also illustrated in figure 3(b). O_3 data was collected by inserting a stainless-steel probe through 0.7 cm circular holes/orifices in the chamber walls and placing it at different points of the plain. The probe was connected to an ozone monitor 2B Technologies model 202. At least three samples were collected at each point of the grid of each plane every 10 s for a period of 5 min. Before starting each experimental run, the test chamber is let to stand with the lid open and O_3 levels are monitored inside it for 15 min to reduce error in O_3 measurements. Both reactors were run at equal power (1.8 W), this was achieved at 13 kVpp/4 kHz, in case of the Fan, and 10.5 kVpp/4 kHz, in case of the Comb.

Both reactors were fabricated with dielectric barriers of hydrocarbon-ceramic (RO4350B) with thickness of 0.76 mm. This composite material has shown very good durability and resistance to chemical corrosion [14] and is more flexible than

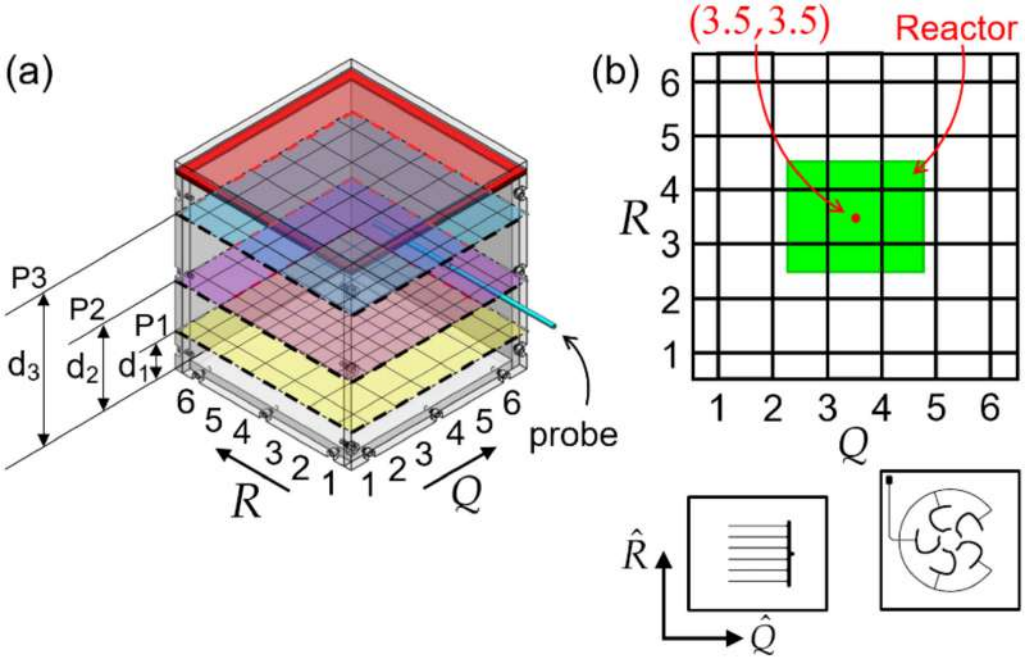

Figure 3. (a) Experimental setup for collection of O_3 samples. (b) 2D grid of 36 measurement points with actuator orientation inlays.

pure ceramics, facilitating the fabrication of the reactors. The electrodes were made of copper with a thickness of 35 μm, and the extra insulation layer covering the bottom electrode was made of Kapton film of the same thickness.

4. Results and discussion

Flow effects of the fan reactor are complex. Therefore, the analysis has been broken down in a step-by-step fashion, starting with the examination of the flow velocity exerted by a single blade and its different segments, followed by the study of the characteristic flow at the center of the Fan, and finalizing with the analysis of the Fan as a whole.

4.1. Aerodynamic flow induced by a single blade of the Fan

The fluid flow of one blade can be understood as the interaction of the individual flows of L_1, L_2 and L_3, whose respective patterns are shown in figure 4(a)–(c). The magnitude of the flow velocity vector is given by $\|\mathbf{V}\| = \sqrt{u^2 + v^2}$, where u represents the horizontal velocity component (x direction) and v represents the vertical velocity component (y direction). As expected, individual lines, having a large radius of curvature, produce a laminar wall-jet flow at any given point near the edge of the exposed electrode. However, the limited radius still creates a subtle pinching effect for L_1 and L_2 that is too weak to induce a surface normal velocity and streamwise vortices like in a serpentine actuator [11], but strong enough to increase the boundary layer's thickness, which is plotted in figure 4(a) and (b). L_1 generated a maximum velocity of 1.59 m s^{-1} at approximately 23.4 mm downstream from the edge of the electrode; whereas L_2, with a more pronounce curvature, produced a maximum velocity of 2.1 m s^{-1}, the highest among all lines, at a much closer distance from the edge of the exposed electrode with a thicker wall-jet formed by the impingement of force vectors. Figure 4(c) shows that plasma along L_3 yields a thin laminar flow that remains close to the dielectric surface similar to any linear actuator, with the difference that the highest velocity spreads throughout a broader region and there is a stronger suction mechanism near the edge of the exposed electrode. This type of flow is the result of force vectors spreading outwards, like in the spreading region of round serpentine actuators [10, 11].

The simultaneous activation of L_1, L_2 and L_3 yields effects of suction and vertical ejection of fluid at the center of the blade, as seen in the flow field images of figure 4(e) and (f), where the velocity magnitude was normalized by the maximum induced velocity of L_2; i.e. $\|\mathbf{V}\|/\|\mathbf{V}\|_{L_2\,\max}$. Figure 4(e) (Plane 1) reveals two major structures: a vortex close to the surface that pulls surrounding fluid towards the center of the blade and a resultant synthetic jet that expel the fluid upward normal to the surface and away from L_2. The view from Plane 2, shown in figure 4(f), indicates that the vortex propagates along the axis perpendicular to L_1 and L_3.

4.2. Aerodynamic flow at the center of the Fan

The direction of the EHD force induced by L_4 is opposite to that induced by L_3, pushing the fluid towards the center of the Fan in a laminar wall-jet pattern as shown in figure 5(a). Therefore, L_4 does not contribute to the flow structures formed at the center of the blades. Instead, when L_4 is powered simultaneously in all five blade-electrodes, the combined action at the center of the Fan pushes the fluid upwards producing a strong vertical jet (synthetic jet effect) whose normalized average velocity is shown in figure 5(c) and (d).

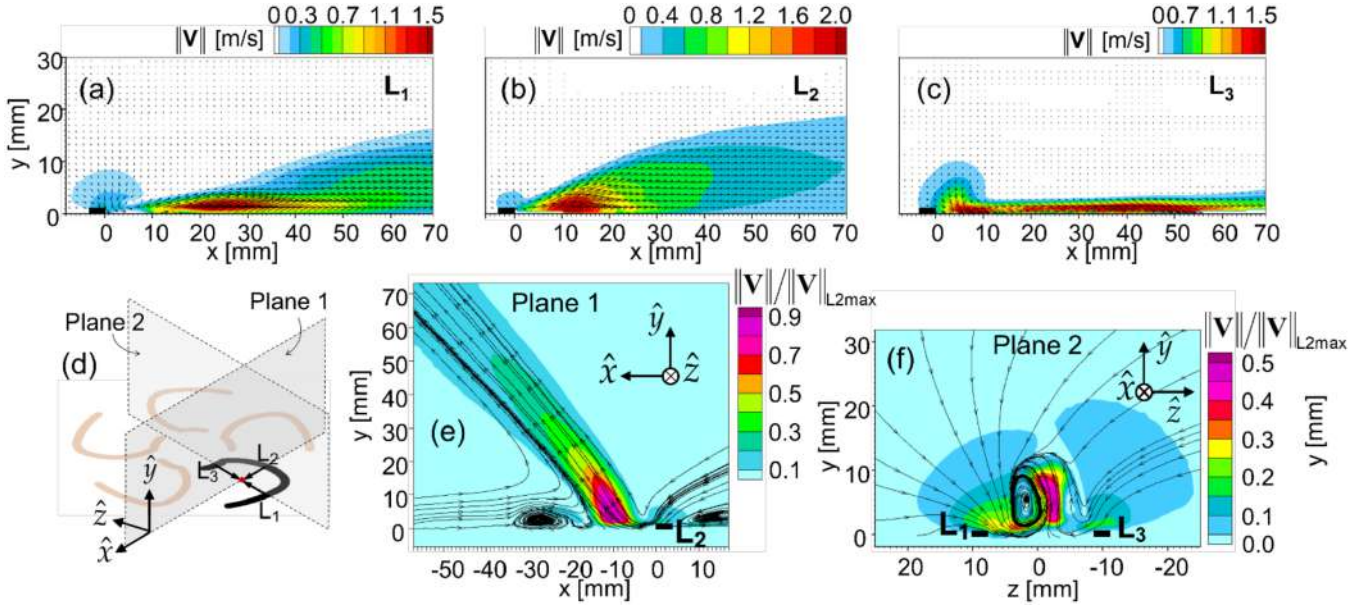

Figure 4. Average velocity induced by a single blade (leg) of the fan reactor. (a)–(c) Fluid flow produced by individual lines L_1, L_2 and L_3. (d) Two view planes for the observation of the overall flow. (e)–(f) Velocity pattern due to interaction of L_1, L_2 and L_3.

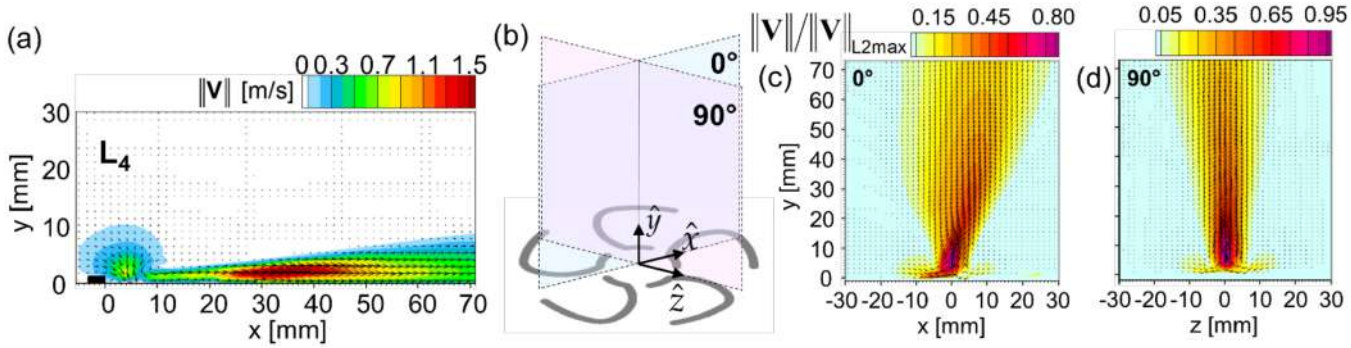

Figure 5. (a) Wall-jet flow produced by a single L_4 line. (b) View planes for the observation of the flow at the center of the Fan. Synthetic jet effect at the center of the reactor created by the interaction of the five L_4 lines on (c) 0° plane and (d) 90° plane.

4.3. Overall flow of the Fan reactor

The overall flow of the fan reactor is presented in figure 6. Smoke flow visualizations in figures 6(a) and (b) show the instantaneous random vortices that develop and disappear as they interact with each other in the Fan's turbulent flow, information that was not possible to obtain with the average velocity shown in figures 6(c) and (d). Figure 6(b) was taken at a higher camera speed to detect vortical structures more clearly. The fluid surrounding the external circumference of the Fan is suctioned by vortical structures formed at the center of each blade. The suction fluid is subsequentially ejected by a jet with an impingement angle. The interaction of the bent jets of the five blades yields a turbulent flow where fluid undergoes irregular and quick fluctuations in both magnitude and direction. In addition, the center of the blade, which is equivalent to a segmented annular ring, pulls fluid from the surface and ejects it in the form of a straight jet which adds energy to the turbulent flow created by the blades. The Fan was configured to have maximum impact on mixing and spreading of the ozonized fluid through the proper manipulation of the EHD force's direction, but also designed to achieve a generous production of ozone and other reactive species.

4.4. Comb reactor

Figure 7 shows the characteristic flow pattern of the comb reactor, which is consistent with other studies [12, 16]. In the side-view of figure 7(b), streamlines indicate that the flow is weak in the area over the Comb. Downstream from the reactor, the movement of fluid gets enhanced due to laminar jets originating from the end (tips) of the teeth. Figures 7(d)–(f) presents three cross-sectional views, one located near the shaft, one located half-way distance between the shaft and the teeth ends, and the third located immediately after the teeth's ends. These images show strong wall-jets originating from the outer edges of the first and sixth teeth of the reactor in the z and $-z$ direction and counterrotating vortex pairs (CVPs) that start forming at the beginning of the teeth, close to the shaft, but

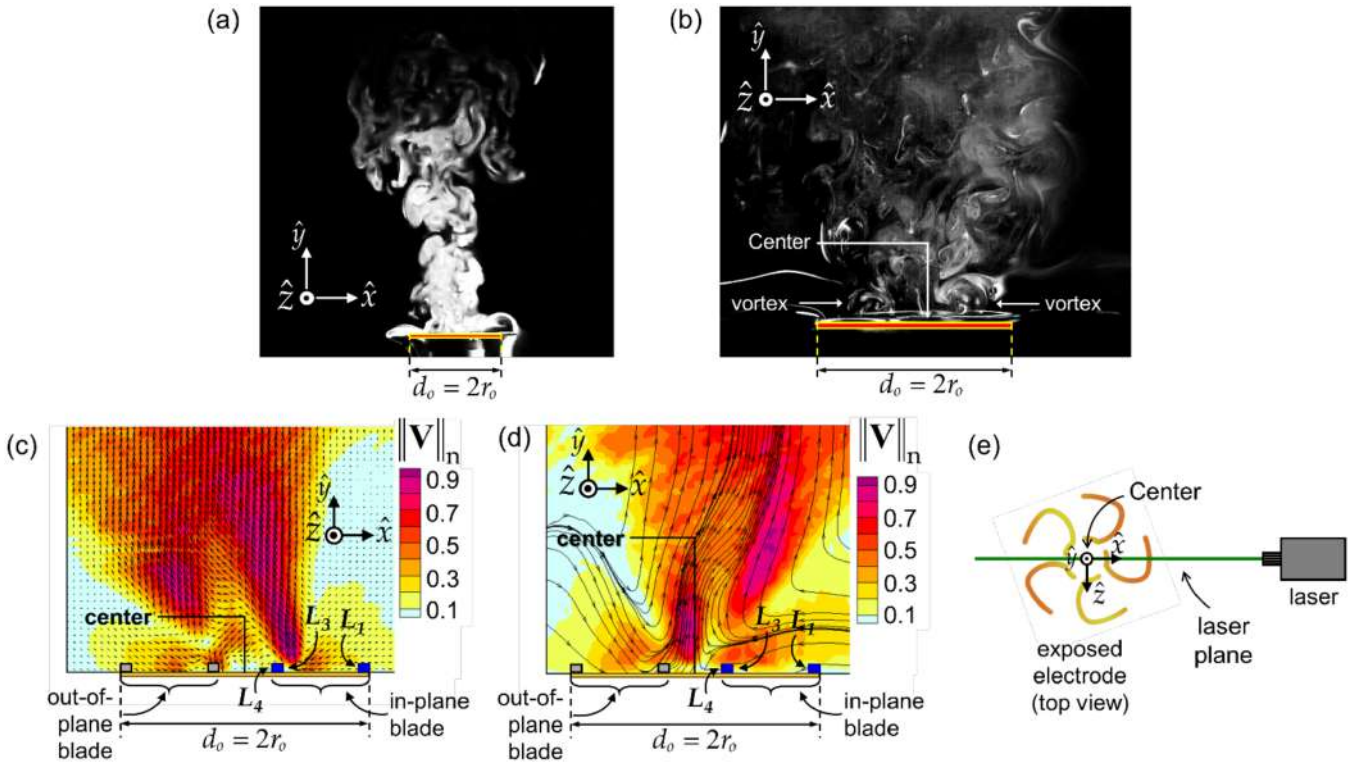

Figure 6. Overall flow pattern of the fan reactor. (a) Smoke flow visualization. (b) Smoke flow visualization at higher camera speed. (c) PIV image showing average velocity. (d) PIV image showing the average velocity and stream traces. (e) Laser plane.

they eventually get disrupted and never fully develop. Some authors [16] concluded that the comb reactor is a special case of square serpentine where strong jets originating at the extremely narrow crest (teeth ends) counteract the momentum of the counterrotating vortices at the narrow pinching region. Furthermore, another factor that can work against the vortices between teeth in the specific case of the comb reactor is the EHD force in the opposite side of the shaft ($-x$ direction), since plasma forms all around the exposed electrode. In summary, the Comb's flow remains close to the surface and is dominated by the downstream wall-jets induced by the teeth ends and the outer edges of the first and sixth teeth as shown figure 7(c).

4.5. Ozone distribution tests

Although the Comb and Fan were run at equal power, plasma regions around the perimeter of the exposed electrode had a larger equivalent length in the case of the Comb. To equalize the average ozone level ($\bar{O}_3$) of both reactors, the ratio $\xi = \text{ave}\,O_{3\,(\text{Fan})}/\text{ave}\,O_{3\,(\text{Comb})}$ was used. This ratio was approximately 0.74, which also coincides with the ratio between the exposed-electrode lengths of the fan and comb reactors. Since the present research focuses on the distribution and not on the amount of O_3 produced, all quantities were normalized. Figure 8(a) shows the graphs of equalized $\bar{O}_3$ for each plane, represented with the notation $[\bar{O}_3]_n$ to indicate it is a normalized quantity. At each time station and for each plane, the standard deviation σ was calculated to measure the diversity or variation of ozone levels at all points of the grid for a given plane. The standard deviation, as presented in figure 8(b), was normalized to eliminate the units of ppm, which is indicated with the symbol σ_n. Although the standard deviation is an indicator of the variation of ozone levels across the plane, this information alone could not determine which reactor design is better at distributing ozone in the decontamination chamber, because the evenness of ozone in the selected plane would not necessarily mean that higher concentrations of ozone are expanding faster. An accurate interpretation of the reactor's performance requires knowledge of the spatial distribution of O_3 along each plane, which was achieved through the color contour graphs shown in figure 9.

According to the transient results plotted for up to 300 s in figure 9(a), the fan reactor generates O_3 levels that grow rapidly from the center of the near-actuation plane P1 toward the outer edges/walls of the box. Contrarily, for the comb reactor, O_3 levels increase more slowly from the edge of the plane P1 toward the center suggesting that the side-walls of the chamber have a dominant role in the mixing process for this design. The scale of turbulent structures induced by the actuation dictates the mixing of ozone at any given region of the enclosure. Since P1 is very close to the actuation force of the reactor, the flow produced by the Fan on this plane is dominated by large turbulent flow structures (figure 6) that yield higher levels but with more random mixing. This explains why the standard deviation is larger for the Fan on this plane. Although it may seem counterintuitive this results in better ozone distribution for fan reactor, since for the Comb the flow is mostly pushed along

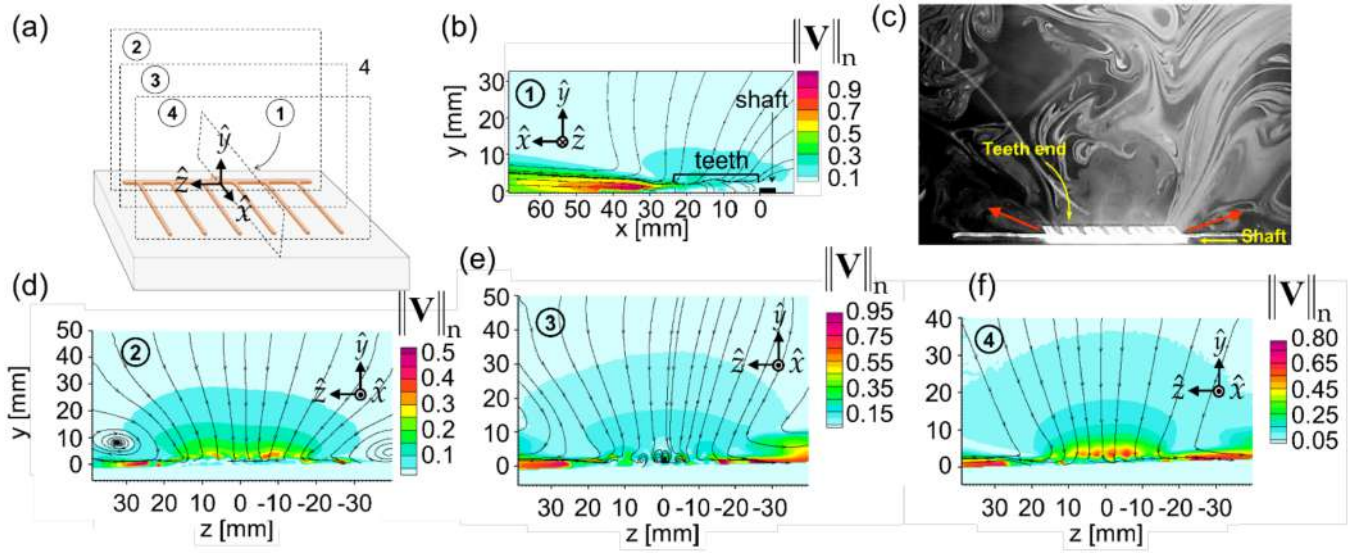

Figure 7. Overall flow pattern of the comb reactor. (a) View planes. (b) Side view. (c) Smoke flow visualization showing the instantaneous behavior of the flow. (d) Cross-sectional view along plane 1. (e) Cross-sectional view along plane 2. (f) Cross-sectional view along plane 3.

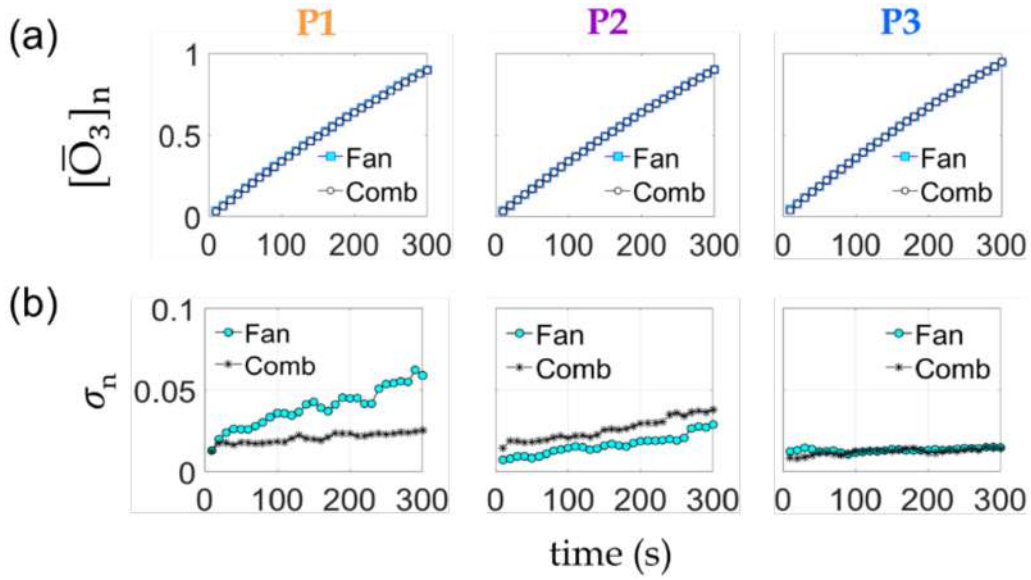

Figure 8. (a) Equalization of $\bar{O}_3$ generated by the fan and comb reactors (normalized). (b) Normalized standard deviation of the measurement samples along each plane.

Table 1. Collected Ozone data for fan and comb reactors in plane P1.

Time	Location	Fan O_3 (ppm)/(R,Q)	Comb O_3 (ppm)/(R,Q)	ΔO_3 (ppm)	ΔO_3 %	Comments
20 s	Center	30.42/(3.5,3.5)	21.32/(3.5,3.5)	9.1	30	Fan O_3 concentration is higher on 66% of P1 area
	Maximum	47.53/(3,4)	43.34/(1,1)	4.2	8.8	
60 s	Center	78.47/(3.5,3.5)	69.53/(3.5,3.5)	8.9	11.4	Fan O_3 concentration is higher on 61% of P1 area
	Maximum	101.97/(3,3)	85.55/(1,3)	16.4	16.1	
150 s	Center	178.38/(3.5,3.5)	167.33/(3.5,3.5)	11.1	6.2	Fan O_3 concentration is higher on 73% of P1 area
	Maximum	203.25/(3,3)	184.80/(1,3)	18.5	9.1	
300 s	Center	323.29/(3.5,3.5)	308.11/(3.5,3.5)	15.2	4.7	Fan O_3 concentration is higher on 70% of P1 area
	Maximum	343.18/(3,3)	325.23/(1,3)	17.9	5.2	

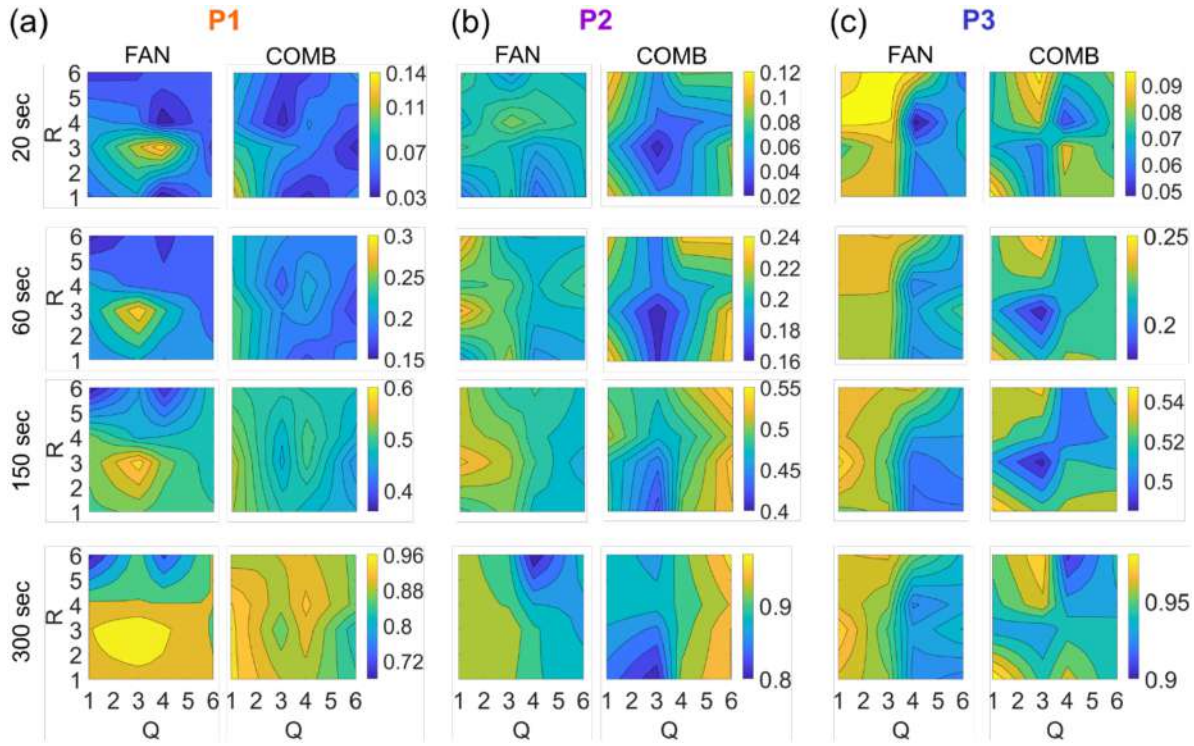

Figure 9. Color contour graphics showing the temporal evolution of normalized O_3 levels on the three transverse planes in the measurement chamber. (a) Color contours for P1. (b) Color contours for P2. (c) Color contours for P3.

the floor toward the sidewall without allowing much mixing (figure 7). This is also supported by the data in table 1 showing higher ozone concentrations for the Fan.

The Fan presents a more uniform O_3 distribution along P2, as indicated by the lower standard deviation seeing in figure 8(b). This happens because the fluid flow that rises in a plume fashion (figure 6) broadens as one moves away from the reactor's surface. This is shown in the color contours corresponding to 20 s in figure 9(b). After 60 s, one can notice that the upward and outward forming swirling flow induced by the fan bounces from the wall further enhancing the mixing process. For the case of the Comb, interactions with the sidewalls seems to be, once more, the main source of mixing. Higher concentrations are located at the corners and the sides; however, the Fan shows a more widespread area of P2 with higher O_3 concentrations (at least >5%). Finally, figure 9(c) shows that at P3 the O_3 distribution for both reactors is highly altered by the interaction with the top and adjacent walls of the box. Still, it is clear that higher O_3 levels cover more area of the plane in the case of the Fan and that the Comb follows the same pattern than in previous planes, where O_3 distribution is dictated by interactions with the walls.

In regard to other reactor configurations like synthetic jets and serpentines that also generate vortical structures, the main advantage is that only the Fan suctions surrounding fluid and ejects it in a turbulent whirl, establishing in a superior ability to effectively mix the O_3 generated with the surrounding fluid. In addition, the turbulent flow rises like a plume with increasing diameter, covering a wider cross-sectional area than what an annular ring would.

5. Conclusion

In summary, a fan shaped plasma reactor was introduced that achieved better ozone distribution in a closed environment than a conventionally used comb shaped reactor. Such distribution was characterized by rapid growth of O_3 levels and random mixing in the lower plane close to the reactor and a more uniform ozone distribution near the mid and high planes of the enclosure, and by higher O_3 concentrations in a larger area for all the planes. With a comb (or other traditional linear electrode) design, the distribution of the generated O_3 in the closed environment is greatly dependent on the reactor orientation and the air flow interactions with the side-walls. This is a great disadvantage in scenarios where the confined volume is much larger than the SDBD reactor. In comparison, the results demonstrate that for the fan reactor mixing of surrounding air with generated O_3 is greatly enhanced. Through a suction mechanism and a combination of neighboring vortical structures, fan reactor yields higher O_3 concentrations and faster spreading from the center of the enclosure. This type of reactor design will be quite suitable for applications where a surface compliant active actuation mechanism is needed in confined spaces such as in a combustor. More studies should be done on optimizing the fan design for specific mixing applications and to ascertain its influence on distribution of other ROS.

Acknowledgments

This research has been partially supported by the Air Force Office of Scientific Research (AFOSR) #FA9550-15-1-0424.

S Portugal wishes to thank the National Research System of the Republic of Panama for their financial and general support. B Choudhury's work was partially funded by an NSF Phase I (IIP 1622071) subcontract through SurfPlasma, Inc.

ORCID iD

Subrata Roy https://orcid.org/0000-0002-2316-0854

References

[1] Khadre M A and Yousef A E 2001 Sporicidal action of ozone and hydrogen peroxide: a comparative study *Int. J. Food Microbiol.* **71** 131–8
[2] Moat J, Cargill J, Shone J and Upton M 2009 Application of a novel decontamination process using gaseous ozone *Can. J. Microbiol.* **55** 928–33
[3] Mastanaiah N, Banerjee P, Johnson J A and Roy S 2013 Examining the role of ozone in surface plasma sterilization using dielectric barrier discharge (DBD) plasma *Plasma Processes Polym.* **10** 1120–33
[4] Shin G A and Sobsey M D 2003 Reduction of Norwalk virus, poliovirus 1, and bacteriophage MS2 by ozone disinfection of water *Appl. Environ. Microbiol.* **69** 3975–8
[5] Hudson J B, Sharma M and Petric M 2007 Inactivation of Norovirus by ozone gas in conditions relevant to healthcare *J. Hosp. Infect.* **66** 40–45
[6] Choudhury B, Portugal S, Mastanaiah N, Johnson J A and Roy S 2018 Inactivation of Pseudomonas aeruginosa and Methicillin-resistant Staphylococcus aureus in an open water system with ozone generated by a compact, atmospheric DBD plasma reactor *Sci. Rep.* **8** 17573
[7] Tipnis N P and Burgess D J 2018 Sterilization of implantable polymer-based medical devices: a review *Int. J. Pharm.* **544** 455–60
[8] Roth J, Sherman D and Wilkinson S 1998 Boundary layer flow control with a one atmosphere uniform glow discharge surface plasma *36th AIAA Aerospace Science Meeting and Exhibit, Reno, Nevada, USA (1998) AIAA Paper* 98–0328
[9] Moreau E, Debien A, Benard N, Jukes T, Whalley R, Choi K, Berendt A, Podliński J and Mizeraczyk J 2013 Surface dielectric barrier discharge plasma actuators *ERCOFTAC Bull.* **94** 5–10
[10] Riherd M and Roy S 2013 Serpentine geometry plasma actuators for flow control *J. Appl. Phys.* **114** 083303
[11] Durscher R J and Roy S 2012 Three-dimensional flow measurements induced from serpentine plasma actuators in quiescent air *J. Phys. D: Appl. Phys.* **45** 035202
[12] Jukes T N and Choi K S 2012 Dielectric-barrier-discharge vortex generators: characterization and optimization for flow separation control *Exp. Fluids* **52** 329–45
[13] Santhanakrishnan A, Reasor D A and LeBeau R P 2009 Characterization of linear plasma synthetic jet actuators in an initially quiescent medium *Phys. Fluids* **21** 043602
[14] Portugal S, Roy S and Lin J 2017 Functional relationship between material properties, applied frequency and ozone generation for surface dielectric barrier discharges in atmospheric air *Sci. Rep.* **7** 6388
[15] Mastanaiah N, Johnson J A and Roy S 2013 Effect of dielectric and liquid on plasma sterilization using dielectric barrier discharge plasma *PLoS One* **8** e708440
[16] Roy S, Zhao P, Das Gupta A and Soni J 2016 Dielectric barrier discharge actuator for vehicle drag reduction at highway speeds *AIP Adv.* **6** 025322
[17] Prasad A K 2000 Stereoscopic particle image velocimetry *Exp. Fluids* **29** 103–16
[18] Yang W J 2001 *Handbook of Flow Visualization* (New York: Taylor & Francis)